CHAPTER II

THEORY

2.1 Spouted-Bed Technique

The spouted-bed technique is a variant of fluidization which is applied to solid materials that are too coarse and uniform in size for good fluidization. The technique is accomplished by forcing fluid flow upwards through a small orifice at the centre of the conical base of the bed column. The particles along the axial zone of the column are then forced to travel upwards and fall downwards in the annular zone. The schematic diagram of a spouted bed is shown in Fig. 2.1 .

2.1.1 Conditions Necessary for Spouting. Stable spouting is dependent on certain parameters: particle size and size distribution, gas-inlet diameter, column diameter, cone angle, gas flow rate, and bed depth. All these factors are interrelated. Unless these are satisfied, the movement of solids become random, leading to a state of aggregate fluidization, and with increase in air flow to slugging.

The conditions necessary for spouting are less serious for coarser particles and for wider columns. In addition, uniformity of particle size favours spouting stability, because the lower permeability of a bed containing a range of sizes would tend to distribute the gas more effectively rather than produce a jet action. Increase in particle size permits the tolerance for size non-uniformity.

The spouting vessel may be either cylindrical or conical in shape.

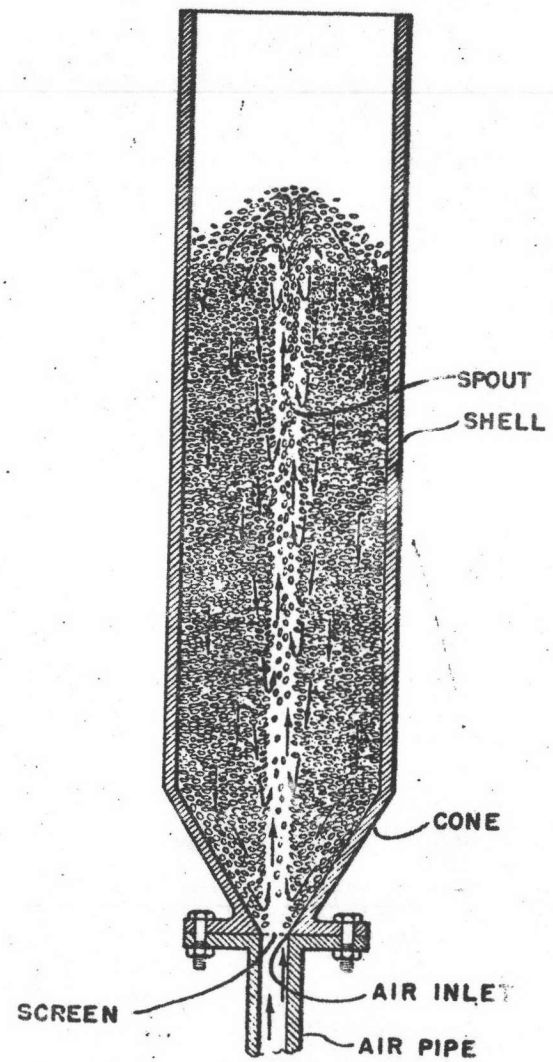

Fig.2.1 Schematic diagram of a spouted bed

The former is preferable to have a short conical base tapering down to the inlet orifice so that the solids in the annulus can slide into the gas- jet region without forming any dead zone at the base. The suitable included angle of the cone depends to some extent on the internal friction characteristics of the solids, but if the cone is too steep, spouting become unstable since the entire bed tends to be lifted up by the air jet. The limiting cone angle for most materials appears to be in region of 40° , both for cylindrical columns with a conical base and for entirely conical vessels. The exact design of the gas-inlet can also have an important effect on spouting stability. More stable spouting is obtained with a converging nozzle slightly protruding into the cone.

2.1.2 Pressure Drop. Spouting causes a pressure gredient (dP/dZ) which is not uniform along the bed height, it is small near the base, increasing to a maximum value at the bed surface. The pressure drop arises from the parallel resistances, that is, the spout in which dilute phase transport of particles is occurring and the annular which is a downward moving packed bed with counter-current flow of gas. The respective pressure drop gradients at various bed levels are in approximate balance, except in the vicinity of the gas inlet. At the top of a deep bed, the pressure gradient approaches that necessary to support the solids, i.e., to fluidize the material. If the gas velocity in the annulus becomes equal to the fluidization. This condition corresponds to the maximum spoutable bed depth.

The total pressure drop across a spouted bed operating at its

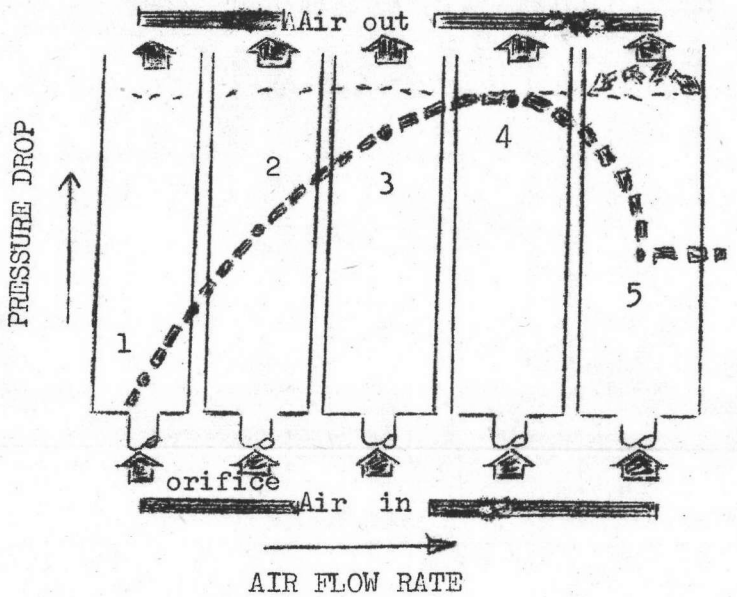

Fig. 2.2 Pressure drop in spouted beds versus air flow rate

Pressure drop curve for spouted bed

Packing

1. Air flows through bed in air jet form-no cavity or internal spout (jet) formation
2. Small cavity opens up near orifice - start or internal solids - air jet. Solid circulation begins in lower cloumn
3. Internal solids - air jet progresses up column
4. Intermal solids - air jet at maximum pressure drop
5. Internal solid - air jet breaks through top of bed. Spouting begins.

maximum depth is approximately equivalent to two-thirds of the weight of the bed, the ratio being lower for shallower bed.

2.1.2.1 Pressure Drop Versus Flow Rate. The change in pressure drop across a bed of rape seed with varying air flow rate is shown pictorially in Fig. 2.2 and graphically in Fig. 2.3.

From Fig 2.3, the high peak in ΔP of curve 1 which occurs before spouting sets in is associated with the entry of a high-velocity gas jet into a bed of solids. Curve 2 shows pressure drop measured separately across the upper part of the same bed (above the cone) while ΔP across the cone itself, obtained by difference, is plotted as curve 3. With increasing air flow, the curve for the upper part remains substantially linear until the spout breaks through the bed (part A). The curve for the lower part rises much more steeply because of the high air velocity near the inlet and goes through a maximum as an internal spout develops in that region. With decreasing air flow, starting with a spouting bed, once the spout has collapsed (point B), ΔP_{upper} follows exactly the same curve as before, but the curve for ΔP_{lower} now sits very much below its previous level since the energy required by the air jet to rupture the solids is no longer expended during the collapse of the interval spout, the pressure drop being entirely due to friction drag.

2.1.2.2 Peak Pressure Drop. To be able to estimate the peak pressure drop is of practical importance for designing the gas-delivery system of the spouting unit. ΔP_{max} as being composed of a rupture

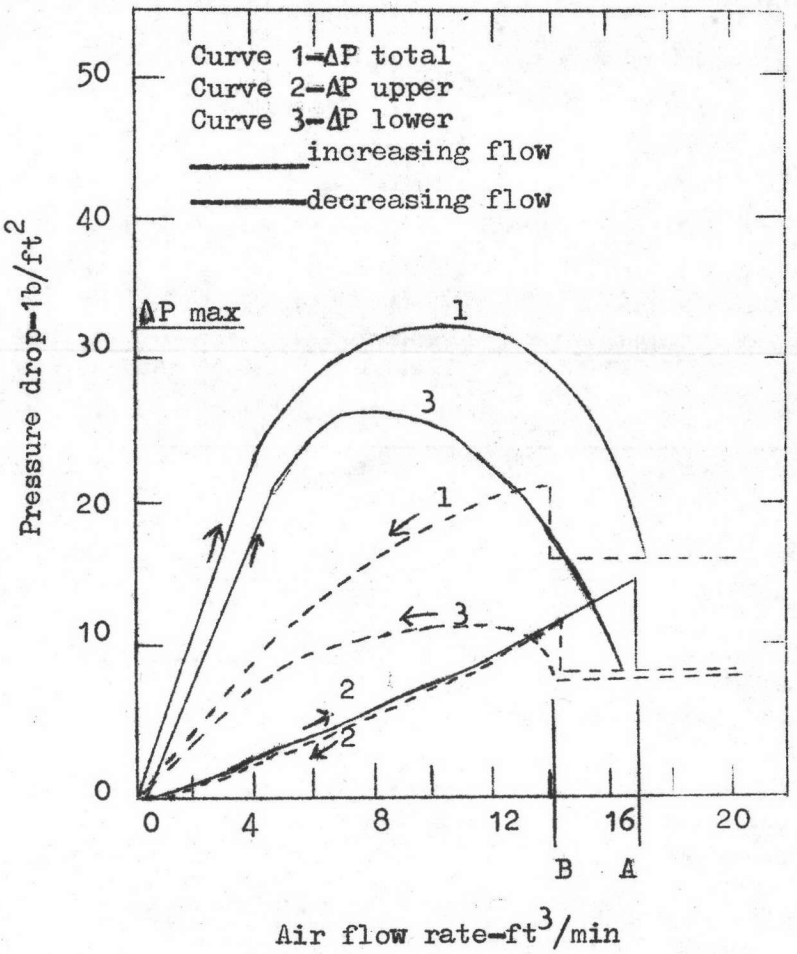

Fig.2.3 Pressure drop versus air flow rate

หอสมุดกลาง จุฬาลงกรณมหาวิทยาลัย

pressure drop and a frictional pressure drop, was experimentally determined and is given in the following correlation:

$$\Delta P_{max} = \left[\frac{6.8}{\tan\alpha} \left(\frac{D_i}{D} \right) + 0.8 \right] H_o \rho_p - 34.4\, d_o \rho_p \qquad (2.1.1)$$

The angle of internal friction, α, was measured by a method given by Zenz and Othmer.

2.1.2.3 Spouting Pressure Drop. Because of the flaring out of gas into the annulus as it travels upwards, the vertical pressure gradient in a spouting bed increases from zero at the base to a maximum near the bed top. The pressure variation with height Z has been found generally to follow a cosine curve:

$$P = \Delta P \cos (\pi Z / 2 H) \qquad (2.1.2)$$

At the maximum spoutable bed depth H_{sm}, the pressure gradient at the top is enough to fluidize the annulus solids, and hence at the top,

$$\frac{dP}{dZ} = - \rho_s \cdot g/g_c \cdot (1 - \varepsilon_o) \qquad (2.1.3)$$

Differentiating equation (2.1.2) with respect to Z and substituting the result into equation (2.1.3) after putting $Z = H = H_{sm}$, we get

$$\Delta P = 2 H_{sm} \cdot \rho_s \cdot g/g_c \cdot (1 - \varepsilon_o) / \pi \qquad (2.1.4)$$

Thus the total spouting pressure drop at H_{sm} bears a ratio of $2/\pi$ (=0.64) to the corresponding value for fluidization. However, the maximum

experimental values reported for this ratio range between 0.7 and 0.8.

2.1.3 Minimum Spouting Velocity. The minimum gas velocity at which a bed will remain in the spouted state depends on solid and fluid properties on the one hand and bed geometry on the other. The following correlation was proposed for cylindrical columns with a short conical base:

$$U_{ms} = \left(\frac{d}{D}\right)\left(\frac{D}{D_i}\right)^{1/3} \sqrt{\frac{2\,g\,H\,(\rho_s - \rho_f)}{\rho_f}} \qquad (2.1.5)$$

For conical vessels, the following form was proposed:

$$Re_{ms} = K \cdot (Ar)^{a} (\tan\gamma)^{b} \left(\frac{H}{D_i}\right)^{c} \qquad (2.1.6)$$

Reynolds number is based on particle diameter and air velocity through the orifice at minimum spouting. The values of the constants and exponents in equation (2.1.6) vary considerably, depending on the range of variables studied.

2.1.4 Maximum Spoutable Bed Depth. Mathur and Gishler found that for the given column, gas and particles, there is a maximum bed depth H_{max} which can be spouted. At bed depths less than this maximum, a stable spout may be maintained at flow rates higher than that required for minumum spouting. But, at the maximum spoutable bed depth, increase in the air flow rate over the minimum spouting causes slugging or aggergative fluidization (Fig. 2.4).

If the minimum fludization velocity for a solid material is known, its maximum spoutable bed depth in a given column can be estimated by substituting U_{mf} for U_{ms} in the minimum spouting velocity equation. For

004637

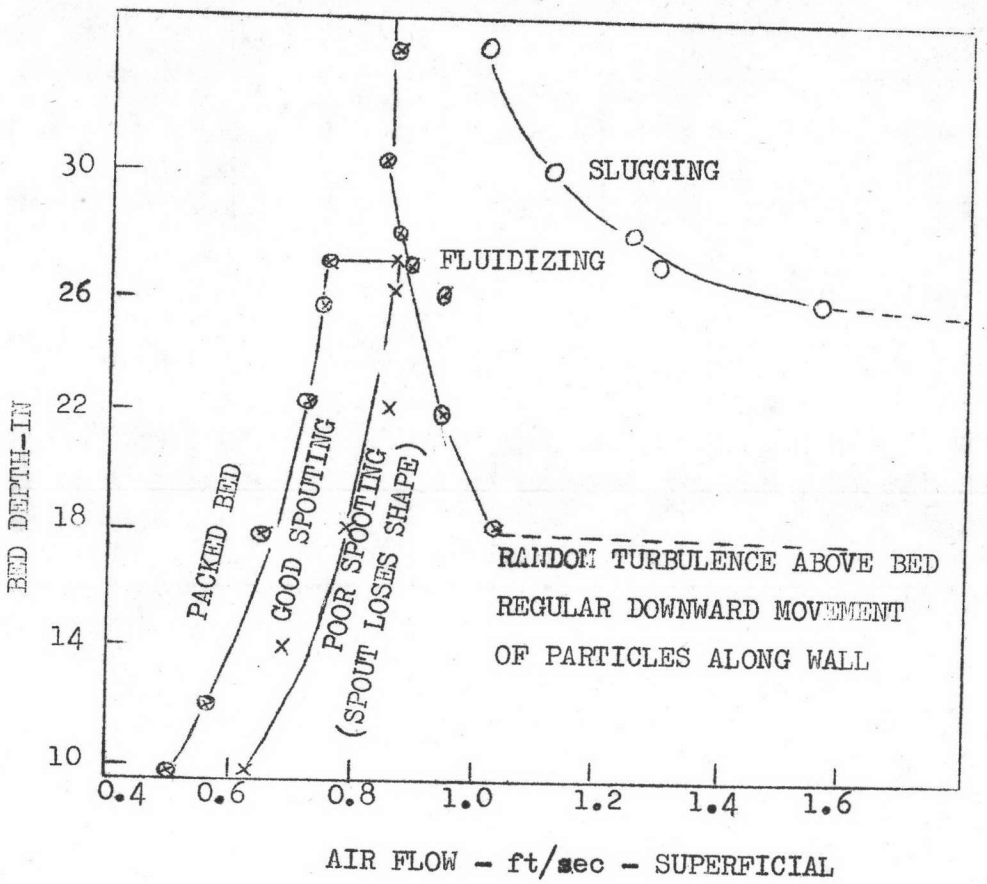

Fig. 2.4 Phase diagram for -20+35 mesh Ottawa sand.
Column diameter=6 in, orifice diameter=0.493 in.

หอสมุดกลาง จุฬาลงกรณมหาวิทยาลัย

i 17350955

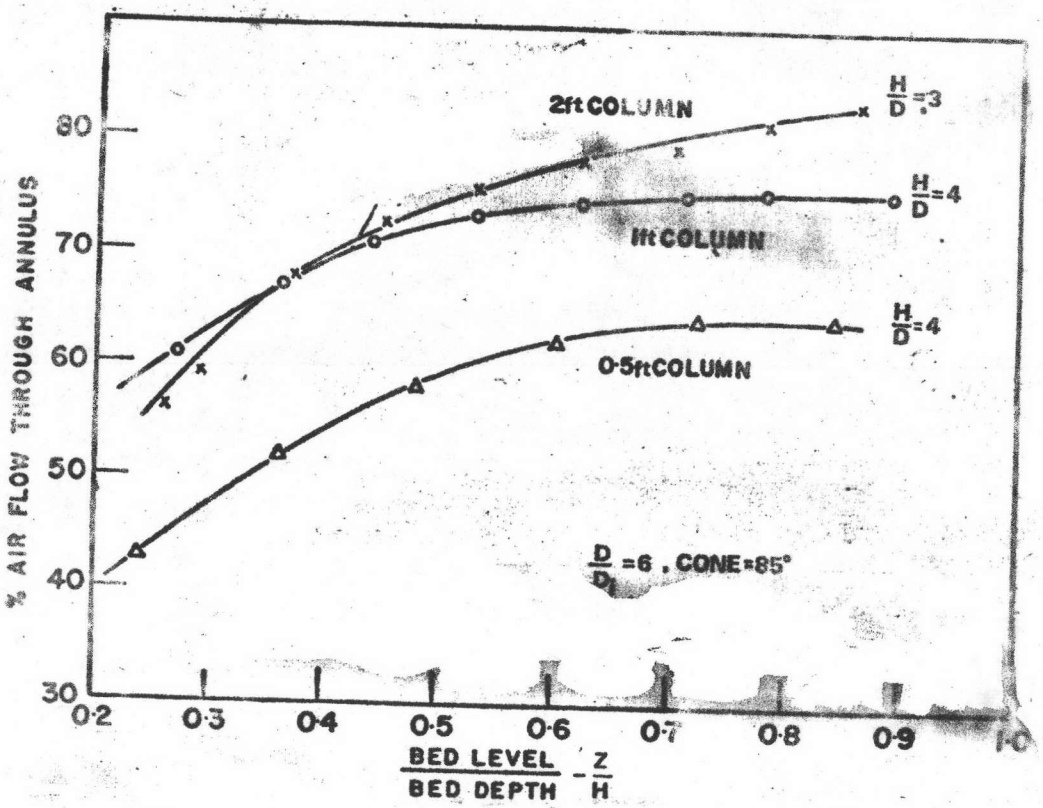

Fig.2.5 Air distribution in spouted wheat beds

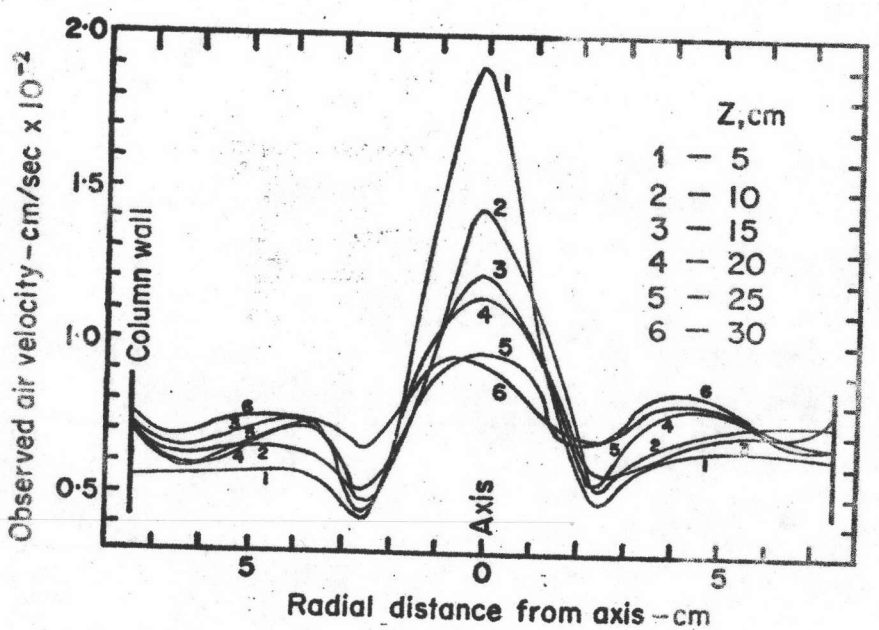

Fig.2.6 Radial profiles of upwards air velocity in a spouted wheat bed (15 cm diameter X 33 cm deep). Air velocity (superficial), 105 cm/sec.

obtaining U_{mf}, it was made use of the Ergun packed bed equation:

$$1.75\ \rho_f d.\ U_{mf}^2 + 150\mu_f\ (\ 1 - \varepsilon_o\ )\ U_{mf} - d^2.\varepsilon_o^3\ \rho_s.\ g = 0 \text{———} (2.1.7)$$

The value of H_{sm} obtained by substituting U_{mf} calculated from equation (2.1.7) into equation (2.1.5) agreed well with experimental results for several closely-sized solids. Attemptes have been made to relate H_{sm} with the variables of the system; however, the above equation is simpler and more accurate.

2.1.5 Flow Pattern of Gas. The distribution of gas between spout and annulus is important in assessing the effectiveness of gas-solids contact.

Fig. 2.5 shows that a substantial proportion of air cross-flows into the annulus within a short distance from the base, the proportion being higher for larger columns. Experiments with 24 in. diameter beds of wheat using different cone angles (45^o - 85^o), inlet diameters (2 in - 4 in.) and air flows (up to 20 % above U_{ms}) showed that the maximum proportion of air passing through the annulus is obtained with a small cone angle, a large orifice size and small air flow rate. At higher flow rates the additional air flows through the spout without spreading into the annulus.

Velecity profiles at several bed levels, determined in a 15 cm diameter X 33 cm deep wheat bed (D_i = 1.4 cm, cone angle = 60^o) are shown in Fig. 2.6.

2.1.6 Flow Pattern of Solids

2.1.6.1 In the Spout. Particles entering the gas jet near the orifice from the annular region accelerate rapidly from rest to a peak velocity within a short distance from the inlet, and then begin to slow down until they reach zero velocity at the spout top. The main accelerating force is due to the frictional drag on the particles by the gas stream, while deceleration is caused by gravity and by collisions between the particles in the spout and those constituting the spout wall. The radial profile of particle velocity in the spout at any level is parabolic, the difference between velocities at the axis and the spout wall decreasing with increasing distance from the air-inlet (Fig. 2.7).

2.1.6.2 In the Annulus. It was observed that a particle starting from any radial position at the bed surface travels down the annulus along an approximately parabolic path, with a radial movement towards the spout. If and when it reaches the lower path of the bed, its path is deflected by the conical base. Thus only for bed levels above the cone region is the downward particle velocity at the circumference of the column similar to the solids velocity across the whole section. In the case of a large column the fraction of total particles which cross-flow into the spout is very much smaller. The flow pattern of gas and solids is shown in Fig. 2.8.

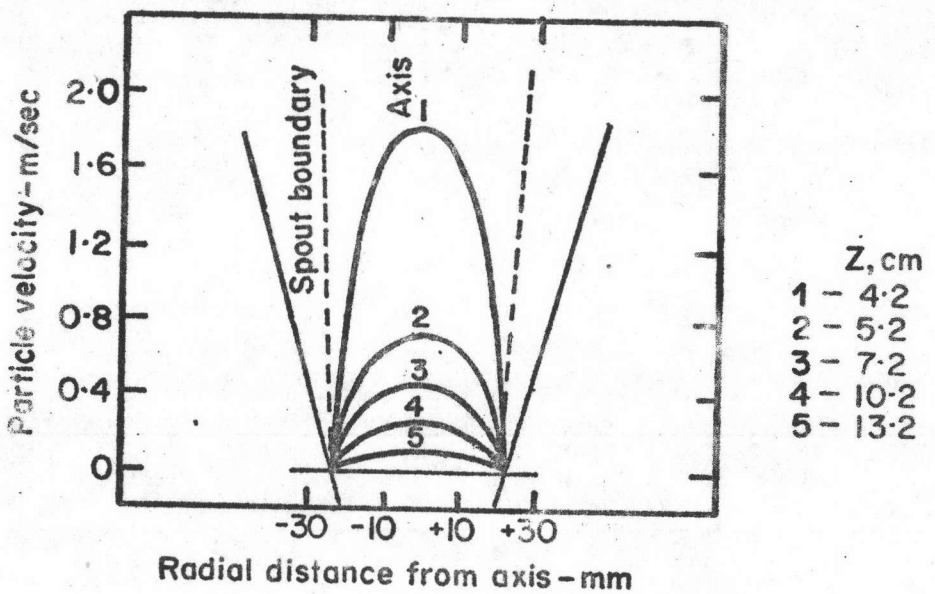

Fig.2.7 Radial profiles of upwards particle in the spout. Conical vessel, $\gamma=30^{0}$, $D_i=4.0$ cm, H=12 cm, d=1.5 mm (catalyst marbles), $u_i=3.47$ m/sec.

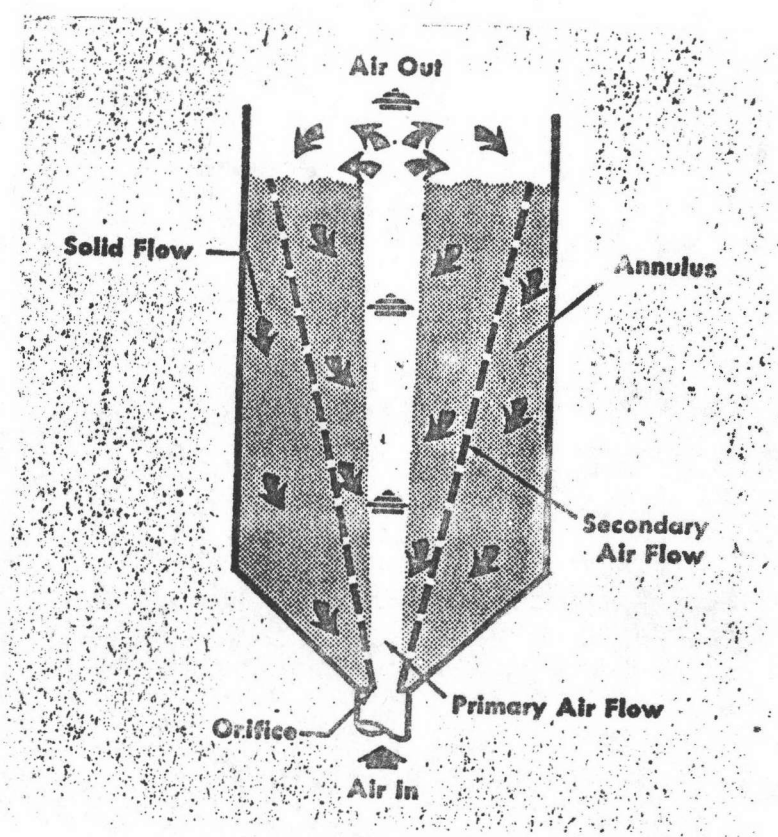

Fig. 2.8 Solid and Air Flows in a Spouted Bed

2.1.7 Cycle Time

Since the proportion of time spent by a particle in the spout is insignificant compared with that spent in the annulus, particle cycle times can be deduced from solids flow in the annulus. The data for wheat in 6 in. to 24 in. diameter columns, H = 24 in. - 72 in., D_i/D_o = 0.17, cone angle = 90° and 180°, were correlated by the following equation:

$$\theta_c = 21 \sqrt{\frac{H}{g}} \cdot \left(\frac{H_{sm}}{D} \right) \qquad (2.1.8)$$

2.2 Mathematical Derivation of Diffusion Drying

Since the drying mechanism of shelled corn[10] is diffusion, and it is assumed that the kernel of corn is a sphere of homogeneous material[11], the following mathematical solution is of unsteady-state molecular diffusion from a sphere.

Assumptions

(a) At the start of diffusion ($\theta=0$), the concentration of moisture (component A) is uniform at C_{AO} throughout the sphere.

(b) The resistance to transfer in the medium surrounding the sphere is negligible, so that the surface concentration of the sphere is constant at C_{AS} in equilibrium with the entire continuous phase.

(c) Diffusion occurs radially, and physical properties are unchanged.

(d) Air humidity is neglected.

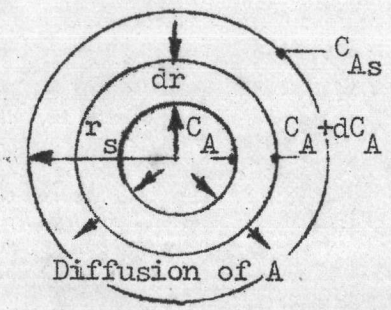

Fig. 2.9 Section of sphere in which mass transfer is occurring by unsteady-state molecular diffusion

Consider the section of a sphere in Fig. 2.9. The origin of coordinates is at the center of the sphere; the concentration at the spherical surface of radius r will be C_A, and at the spherical surface of

radius r+dr it will be C_A+dC_A . A control volume is defined as bounded by these two surfaces at r and r+dr.

The rate of moisture input is

$$-\mathcal{D}(4\pi r^2)\frac{\partial C_A}{\partial r} \qquad (2.2.1)$$

and the rate of moisture output is

$$-\mathcal{D}\left[4\pi(r+dr)^2\right]\left[\frac{\partial C_A}{\partial r}+\frac{\partial}{\partial r}\left(\frac{\partial C_A}{\partial r}\right)dr\right] \qquad (2.2.2)$$

Subtracting equation (2.2.2) from equation (2.2.1) and neglecting second- and third-order differentials gives

$$4\pi\mathcal{D}\left(r^2\frac{\partial^2 C_A}{\partial r^2}dr+2r\frac{\partial C_A}{\partial r}dr\right) \qquad (2.2.3)$$

Equation (2.2.3) is the net flow rate of moisture into the control volume. The rate of cumulation of moisture in the control volume is

$$(4\pi r^2 . dr)\frac{\partial C_A}{\partial \theta} \qquad (2.2.4)$$

Then the mass balance around the control volume is obtained by equating the expressions (2.2.3) and (2.2.4). The result is

$$\frac{\partial C_A}{\partial \theta} = \mathcal{D}\left(\frac{\partial^2 C_A}{\partial r^2}+\frac{2}{r}\cdot\frac{\partial C_A}{\partial r}\right) \qquad (2.2.5)$$

with the boundary conditions following from the assumptions:

$$C_A(r,0) = C_{AO}$$

$$C_A(r_s,\theta) = C_{As}$$

$$\lim_{r\to 0} C_A(r,\theta) = \text{bounded}$$

where r_s is radius of the sphere.

In order to simplify the boundary conditions, the change of variable

$$y = C_A - C_{As}$$

is made. Then equation (2.2.5) becomes

$$\frac{\partial y}{\partial \theta} = \mathcal{D}\left(\frac{\partial^2 y_2}{\partial r^2} + \frac{2}{r}\frac{\partial y}{\partial r}\right) \qquad (2.2.6)$$

with the boundary conditions

$$y\,(r,0) = C_{AO} - C_{As} \qquad (2.2.7\ a)$$

$$y\,(r_s,\theta) = 0 \qquad (2.2.7\ b)$$

$$\lim_{r \to \infty} y\,(r,\theta) = \text{bounded} \qquad (2.2.7\ c)$$

Assume that the solution of equation (2.2.6) is of the form

$$y\,(r,\theta) = R(r)\,T(\theta) \qquad (2.2.8)$$

where R (r) is some function of r only, and T (θ) is some function of θ only.

Then

$$\frac{\partial y}{\partial \theta} = R\frac{dT}{d\theta}$$

$$\frac{\partial y}{\partial r} = T\frac{dR}{dr}$$

$$\frac{\partial^2 y_2}{\partial r} = T\frac{d^2 R_2}{d\,r}$$

and equation (2.2.8) becomes

$$\frac{1}{\mathcal{D}T}\frac{dT}{d\theta} = \frac{1}{R}\left(\frac{d^2 R_2}{dr} + \frac{2}{r}\cdot\frac{dR}{dr}\right) = -\lambda^2 \qquad (2.2.9)$$

where $-\lambda^2$ is a constant.

Solving the first differential equation gives

$$T = C_1 \exp\left(-\lambda^2 \mathcal{D}\theta\right) \qquad (2.2.10)$$

The second differential equation is

$$\frac{d^2R}{dr^2} + \frac{2}{r}\frac{dR}{dr} + \lambda^2 R = 0 \qquad (2.2.11)$$

Let $rR = \beta$, then

$$\frac{dR}{dr} = -\frac{\beta}{r^2} + \frac{1}{r}\frac{d\beta}{dr} \qquad (2.2.12)$$

$$\frac{d^2R}{dr^2} = \frac{2\beta}{r^3} - \frac{2}{r^2}\frac{d\beta}{dr} + \frac{1}{r}\frac{d^2\beta}{dr^2} \qquad (2.2.13)$$

Substituting equations (2.2.12) and (2.2.13) into equation (2.2.11) gives

$$\frac{d^2\beta}{dr^2} + \lambda^2\beta = 0$$

This equation has the solution of the form

$$\beta = C_2 \sin \lambda r + C_3 \cos \lambda r$$

from which

$$R = \frac{C_2}{r} \sin \lambda r + \frac{C_3}{r} \cos \lambda r \qquad (2.2.14)$$

The boundary condition (2.2.7 b) for R to be finite at r = 0 requires

$$C_3 = 0$$

Also, from the boundary condition (2.2.7 b) and equation (2.2.8),

$$R(r = r_s) = 0 = \frac{C_2}{r_s} \sin \lambda r_s \qquad (2.2.15)$$

Therefore

$$\lambda = \frac{n\pi}{r_s} \qquad (2.2.16)$$

หอสมุดกลาง จุฬาลงกรณมหาวิทยาลัย

where $n = 1,2,3,- - -$

$$R = \frac{C_2}{r} \sin\left(\frac{n \pi r}{r_s}\right) \qquad (2.2.17)$$

Substituting equations (2.2.10) and (2.2.17) into equation (2.2.8), we obtain

$$y = \sum_{n=1}^{\infty} A_n \cdot \frac{1}{r} \sin\left(\frac{n \pi r}{r_s}\right) \exp\left(\frac{-\mathcal{D} n^2 \pi^2}{r_s^2}\right) \qquad (2.2.18)$$

The boundary condition (2.2.7 a), for $y = C_{Ao} - C_{As}$ at $\theta = 0$ gives

$$r (C_{Ao} - C_{As}) = \sum_{n=1}^{\infty} A_n \sin\left(\frac{n \pi r}{r_s}\right) \qquad (2.2.19)$$

This is a Fourier sine series for $f(r) = r(C_{Ao} - C_{As})$, so that A_n may be evaluated as follows:

$$A_n = \frac{2}{r_s} \int_0^{r_s} r(C_{Ao} - C_{As}) \sin\left(\frac{n \pi r}{r_s}\right) dr$$

$$= \frac{2r_s}{n \pi} (C_{Ao} - C_{As}) (-1)^{n+1} \qquad (2.2.20)$$

Then equation (2.2.18) becomes

$$C_A = C_{As} + \frac{2}{\pi} r_s (C_{Ao} - C_{As}) \sum_{n=1}^{\infty} \frac{(-1)^{n+1}}{n} \cdot \frac{1}{r} \sin\left(\frac{n \pi r}{r_s}\right) \exp\left(-\mathcal{D} n^2 \pi^2 \theta / r_s^2\right) \qquad (2.2.21)$$

Evaluating $\frac{\partial C_A}{\partial r}$ at $r = r_s$ from equation (2.2.21) gives

$$\left(\frac{\partial C_A}{\partial r}\right)_{r = r_s} = -\frac{2}{r_s} (C_{Ao} - C_{As}) \sum_{n=1}^{\infty} \exp\left(-\mathcal{D} n^2 \pi^2 \theta / r_s^2\right) \qquad (2.2.22)$$

The rate of mass transfer at time θ across the surface of the sphere is

$$4\pi r_s^2 N_{Ar}(\theta) = -4\pi r_s^2 \mathcal{D}\left(\frac{\partial C_A}{\partial r}\right)_{r = r_s} \qquad (2.2.23)$$

Substituting equation (2.2.22) into equation (2.2.23) gives

$$4\pi r_s^2 N_{Ar}(\theta) = 8\pi r_s \mathcal{D} (C_{Ao} - C_{As}) \sum_{n=1}^{\infty} \exp\left(\frac{-\mathcal{D} n^2 \pi^2 \theta}{r_s^2}\right) \qquad (2.2.24)$$

The total mass transfer up to time θ is N_A', where

$$N_A' = 4\pi r_s^2 \int_0^{\theta} N_{Ar}(\theta)\, d\theta$$

$$= \frac{8 r_s^2}{\pi} (C_{Ao} - C_{As}) \sum_{n=1}^{\infty} \frac{1}{n^2}\left[1 - \exp\left(\frac{-\mathcal{D} n^2 \pi^2 \theta}{r_s^2}\right)\right] \qquad (2.2.25)$$

The total transfer per unit surface up to time θ is

$$\frac{N_A'}{4\pi r_s^2} = (C_{Ao} - C_{As}) \frac{r_s}{3}\left[\frac{6}{\pi^2} \sum_{n=1}^{\infty} \frac{1}{n^2} - \frac{6}{\pi^2} \sum_{n=1}^{\infty} \frac{1}{n^2} \exp\left(\frac{-\mathcal{D} n^2 \pi^2 \theta}{r_s^2}\right)\right] \qquad (2.2.26)$$

where it can be shown that

$$\sum_{n=1}^{\infty} \frac{1}{n^2} = \frac{\pi^2}{6} \qquad (2.2.27)$$

Substituting equation (2.2.27) into equation (2.2.26) gives

$$\frac{N_A'}{4\pi r_s} = (C_{Ao} - C_{As})\frac{r_s}{3}\left[1 - \frac{6}{\pi^2}\sum_{n=1}^{\infty}\frac{1}{n^2}\exp\left(\frac{-\mathcal{D}n^2\pi^2\theta}{r_s^2}\right)\right] \qquad (2.2.28)$$

A material balance on the transfer up to time θ is

$$(C_{Ao} - \bar{C}_A)\frac{4}{3}\pi r_s^3 = N_A' \qquad (2.2.29)$$

in which $\bar{C}_A$ is the average concentration throughout the sphere at θ.

Substitution of equation (2.2.28) into equation (2.2.29) and rearrangement give

$$\frac{C_{Ao} - \bar{C}_A}{C_{Ao} - C_{As}} = \frac{3N_A'}{4\pi r_s^3 (C_{Ao} - C_{As})} = 1 - \frac{6}{\pi^2}\sum_{n=1}^{\infty}\frac{1}{n^2}\exp\left(\frac{-\mathcal{D}n^2\pi^2\theta}{r_s^2}\right) \qquad (2.2.30)$$

The results similar to that obtained by Becker, Hall, and Hustrulid[11] are in terms of error functions and associated functions as follows:[13]

$$\bar{C}_A = C_{Ao} + \frac{r_s}{r}(C_{As} - C_{Ao})\sum_{n=0}^{\infty}\left[\operatorname{erfc}\frac{(2n+1)r_s - r}{2\sqrt{\mathcal{D}\theta}} - \operatorname{erfc}\frac{(2n+1)r_s + r}{2\sqrt{\mathcal{D}\theta}}\right] \qquad (2.2.31)$$

and

$$\frac{C_{Ao} - \bar{C}_A}{C_{Ao} - C_{As}} = 6\sqrt{\frac{\mathcal{D}\theta}{r_s^2}}\left[\frac{1}{\sqrt{\pi}} + 2\sum_{n=1}^{\infty}\operatorname{ierfc}\frac{nr_s}{\sqrt{\mathcal{D}\theta}}\right] - 3\frac{\mathcal{D}\theta}{r_s^2} \qquad (2.2.32)$$

where

$$\operatorname{erf}\xi = \frac{2}{\sqrt{\pi}}\int_0^{\xi}\exp(-\eta^2)d\eta$$

in which η is any "dummy" variable, used merely to describe the function to be integrated.

$$\text{erfc } \xi = \frac{2}{\sqrt{\pi}} \int_{\xi}^{\infty} \exp(-\eta^2)\, d\eta = 1 - \text{erf } \xi$$

$$\text{ierfc } \xi = \int_{\xi}^{\infty} \text{erfc}\, \eta\, d\eta = \frac{1}{\sqrt{\pi}} \exp(-\xi^2) - \xi\, \text{erfc}\, \xi$$

Let

$$X = \frac{S}{V} \sqrt{\mathcal{D}\theta}$$

where $\frac{V}{S}$ is the volume - to - surface ratio. For the sphere, $\frac{V}{S} = \frac{r_s}{3}$ (4).

Then

$$X = \frac{S}{V}\sqrt{\mathcal{D}\theta} = \frac{3\sqrt{\mathcal{D}\theta}}{r_s} \qquad (2.2.33)$$

Therefore, equation (2.2.32) becomes

$$\frac{\bar{C}_{Ao} - \bar{C}_A}{C_{Ao} - C_{As}} = 2X \left[\frac{1}{\sqrt{\pi}} + 2 \sum_{n=1}^{\infty} \text{ierfc } \frac{3n}{X} \right] - \frac{1}{3} X^2 \qquad (2.2.34)$$

For $X \Rightarrow 0$, we obtain, from equation (2.2.34)

$$\frac{\bar{C}_{Ao} - \bar{C}_A}{C_{Ao} - C_{As}} \Longrightarrow \frac{2}{\sqrt{\pi}} X$$

where $\text{erf}(0) = 0$

and $\text{erf}(\infty) = 1$ (12)

Let

$$\bar{C} = 1 - \frac{\bar{C}_{Ao} - \bar{C}_A}{C_{Ao} - C_{As}} = \frac{\bar{C}_A - C_{As}}{C_{Ao} - C_{As}} \qquad (2.2.35)$$

Then $\bar{C} \Rightarrow 1 - \frac{2}{\sqrt{\pi}} X$ as $X \Rightarrow 0$ (2.2.36)

or

$$\frac{1 - \bar{C}}{X} = \frac{2}{\sqrt{\pi}} \qquad \text{at} \quad X = 0 \tag{2.2.37}$$

This result[4] gives a first approximation to a general solution, valid in the neighborhood of $\theta = 0$, of the nonsteady-state differential diffusion equation. Note that the prescribed form of the solution for $\theta > 0$ is

$$\bar{C} = f(X) \tag{2.2.38}$$

To obtain a more accurate approximation, we assume that $f(X)$ can be represented, in the neighborhood of $X=0$, as a power series in X; we find, (Maclaurin's series):

$$f(y) = f(0) + f'(0)\,X + \frac{f''(0)}{2!}X^2 + - - - - - + \frac{f^n(0)}{n!}X^n \tag{2.2.39}$$

From equation (2.2.36), we obtain

$$f(0) = 1 \tag{2.2.40}$$

$$\text{and} \quad f'(0) = -\frac{2}{\pi} \tag{2.2.41}$$

The higher derivatives, $f''(0)$, etc., are dependent on solid shape[4]. However, since the series should converge rapidly near $X=0$, terms higher than $f''(0)$ will be neglected, giving for our final approximation

$$\bar{C} = 1 - \frac{2}{\sqrt{\pi}}X + \frac{f''(0)}{2!}X^2 \tag{2.2.42}$$

Equation (2.2.42) was derived for a solid of constant dimensions. For such a solid, $\bar{C}$ is exactly equal to $\bar{M}$, where

$$\bar{M} = (\bar{m} - m_s) / (m_o - m_s) \tag{2.2.43}$$

However, in most natural and synthetic polymers, moisture adds its volume (as liquid water) to the volume of the solid. Since it is not practicable to account for the resulting swelling, it must be assumed that $\bar{C} = \bar{M}$ in these cases also. The resulting error should not be serious so long as $(m_o - m_s)$ is reasonably small compared with the specific volume of the solid (in cm^3/g).(4) Then equation (2.2.42) becomes

$$\bar{M} = 1 - \frac{2}{\sqrt{\pi}} X + \frac{f''(0)}{2!} X^2 \qquad (2.2.44)$$

Equation (2.2.44) was derived for a drying particle.

Let

$$\bar{\bar{M}} = (\bar{\bar{m}} - m_s) / (m_o - m_s) \qquad (2.2.45)$$

wher $\bar{\bar{m}}$ = average moisture content of a statistical population of drying particles.

Therefore, equation (2.2.44) becomes

$$\bar{\bar{M}} = 1 - \frac{2X}{\sqrt{\pi}} + \frac{f''(0)}{2!} X^2 \qquad (2.2.46)$$

Substitution of $\bar{M} = (\bar{\bar{m}} - m_s) / (m_o - m_s)$ and $X = \frac{S}{\bar{V}}\sqrt{\mathcal{D}\theta}$ into equation (2.2.45) gives

$$\frac{\bar{\bar{m}} - m_s}{m_o - m_s} = 1 - \frac{2}{\sqrt{\pi}} \cdot \frac{S}{\bar{V}}\sqrt{\mathcal{D}\theta} + \frac{f''(0)}{2!}\left(\frac{S}{\bar{V}}\right)^2 \mathcal{D}\theta \qquad (2.2.47)$$

Upon rearrangement, equation (2.2.46) becomes

$$\frac{m_o - \bar{\bar{m}}}{m_o - m_s} = \frac{2}{\sqrt{\pi}} \cdot \frac{S}{\bar{V}}\sqrt{\mathcal{D}\theta} - \frac{f''(0)}{2!}\left(\frac{S}{\bar{V}}\right)^2 \mathcal{D}\theta \qquad (2.2.48)$$

Multiplying equation (2.2.46) by $(m_o - m_s)/\sqrt{\theta}$, we get

$$\frac{m_o - \bar{\bar{m}}}{\sqrt{\theta}} = \frac{2}{\sqrt{\pi}} \cdot \frac{S}{V} \sqrt{\mathcal{D}}(m_o - m_s) - \frac{f''(0)}{2!}\left(\frac{S}{V}\right)^2 \mathcal{D}(m_o - m_s)\sqrt{\theta} \quad (2.2.49)$$

Since $$\frac{V}{S} = \frac{r_s}{3} \cdot \frac{4\pi r_s^2}{S} \quad (2.2.50)$$

and the factor $4\pi r_s^2 / S$ is a shape factor commonly known as the sphericity and denoted by ψ, then equation (2.2.49) becomes

$$\frac{V}{S} = \frac{r_s \psi}{3} \quad (2.2.51)$$

Substituting equation (2.2.50) into equation (2.2.48) gives

$$\frac{m_o - \bar{\bar{m}}}{\sqrt{\theta}} = \frac{2}{\sqrt{\pi}} \cdot \frac{3}{r_s \psi} \sqrt{\mathcal{D}}(m_o - m_s) - \frac{f''(0)}{2!}\left(\frac{3}{r_s \psi}\right)^2 \mathcal{D}(m_o - m_s)\sqrt{\theta} \quad (2.2.52)$$

For convenience, equation (2.2.51) is reduced to

$$k = k_o - b\sqrt{\theta} \quad (2.2.53)$$

This equation is similar to that obtained by Becker.[4]

where

$$k = \frac{m_o - \bar{\bar{m}}}{\sqrt{\theta}} \quad (2.2.54)$$

$$k_o = \frac{2}{\sqrt{\pi}} \cdot \frac{3}{r_s \psi} \cdot \sqrt{\mathcal{D}}(m_o - m_s) \quad (2.2.55)$$

and $$b = \frac{f''(0)}{2!}\left(\frac{3}{r_s \psi}\right)^2 \mathcal{D}(m_o - m_s) \quad (2.2.56)$$

It is shown that equation (2.2.52) is a straight line equation with intercept k_o and slope $-b$.

The experiment is to be performed to evaluate $f''(0)$ from experimental values of m_o, $\bar{\bar{m}}$, and θ.